

Thermodynamic behavior and polymorphism of 1-butyl-3-methylimidazolium hexafluorophosphate composites with multiwalled carbon nanotubes

Tatsiana Liavitskaya^{1,2}, Eugene Paulechka^{1,3*}, Andrey V. Blokhin¹, and Marina Shevelyova^{1,4}

¹ *Chemistry Faculty, Belarusian State University, 220030 Minsk, Belarus*

² *Department of Chemistry, University of Alabama at Birmingham, Birmingham, AL 35294-1240, United States*

³ *Applied Chemicals and Materials Division, National Institute of Standards and Technology, Boulder, CO 80305-3337, United States*

⁴ *Protein research group, Institute for Biological Instrumentation of the Russian Academy of Sciences, Pushchino, Moscow region, 142290 Russia*

* To whom correspondence should be addressed. E-mail: yauheni.paulechka@nist.gov

Abstract

Based on room-temperature densities measured in this research for ionic nanofluids (INFs) with four ionic liquids (ILs), we conclude that evacuation is a necessary step to maximize the IL penetration into multiwalled carbon nanotubes (MWCNT). An improved procedure for reproducible preparation of INFs is proposed. Thermal behavior of five (1-butyl-3-methylimidazolium hexafluorophosphate + MWCNT) samples was studied by adiabatic calorimetry over the temperature range (78 to 370) K. The samples contained from 0.11 to 0.92 mass fraction of the nanophase. Their appearance changed from the fluid to the powder with increasing the MWCNT content. For the fluid samples, the specific heat capacity was found to be an additive quantity of the specific heat capacities of the components for the crystal and liquid phases, and the temperatures of phase transitions did not change relative to the bulk values. For the powder-like sample with the highest IL content, a sigmoidal heat capacity curve was observed. Thus, the internal diameter of the studied MWCNT was small enough to switch from the isothermal melting process to the gradual transition from the crystal-like structures to the liquid-like ones.

1. Introduction

This work continues our activities on thermodynamic characterization of ionic liquid (IL) materials with multiwalled carbon nanotubes (MWCNT) [1]. Experimental thermodynamic studies of the materials that contain a liquid interacting with a nanophase (NP) typically consider two aspects: (1) heat capacity of these systems and their constituents, and (2) a change of fusion or glass-transition parameters - primarily temperatures - for the liquid adsorbed on the NP surface.

Previously [1], we reviewed the available experimental data on heat capacity of nanofluids (NF). Significant inconsistencies and experimental problems were identified. It was noted that such measurements need to be performed using methods with small uncertainty ($<0.01 c_P$), such as adiabatic or Calvet-type calorimetry. These instruments are accurate enough to conclusively detect anomalies in the heat capacity, if present.

If an IL is used as a base fluid, the resulting NF is often termed an *ionic nanofluid* (INF). Our measurements with adiabatic calorimetry for the INF of (MWCNT + 1-butyl-methylimidazolium hexafluorophosphate [C_4mim] PF_6) and (MWCNT + 1-butyl-3-methylimidazolium tetrafluoroborate [C_4mim] BF_4) [1] did not reveal any statistically significant deviation from the equation:

$$c_P(INF) = c_P(liq) (1 - w(NP)) + c_P(NP) w(NP) \quad (1)$$

where $w(NP)$ is the mass fraction of NP, c_P represents the specific heat capacity.

Subsequently, three papers [2, 3, 4] were published that claimed a significant increase of INF heat capacity relative to the pure IL. Liu et al. [2] reported the heat capacity of [C_6mim] BF_4 composites with graphene, and Paul et al. [3] studied INFs of Al_2O_3 with [C_4mim] NTf_2 and

[C₄mPr]NTf₂. The heat capacities of the base IL in both works were about $0.3c_P$ higher than the evaluated values [5]. Therefore, no conclusion about consistency of these results with eq. (1) can be made.

Oster et al. [4] measured c_P for INFs with many ILs containing up to 0.03 mass fraction of MWCNT, boron nitride, or graphite. Despite the small NP content, the specific heat capacities of the INFs were as much as $0.28c_P$ higher than those of the neat ILs. The measured heat capacities of ILs deviated from the evaluated values [5] by up to $0.09c_P$. Using the average geometrical parameters of the MWCNT [4], one can roughly estimate a specific surface area for this material to be $170 \text{ m}^2 \cdot \text{g}^{-1}$. If one assumes that an ionic pair occupies $\sim 0.4 \text{ nm}^2$ on the MWCNT surface, a monolayer of adsorbed IL, for example, [C₄mim]N(CN)₂, will contain $<0.14 \text{ g}$ of IL per 1 g of NP. For $w(\text{NP}) = 0.03$, it corresponds to 0.004 mass fraction of IL directly interacting with MWCNT. Even if this interaction affects several layers of ions, the heat capacity change for these layers would need to be extremely large to explain the experimental results.

Another important thermodynamic parameter that characterizes properties of nanosized systems is the temperature of fusion T_{fus} of a nanoconfined liquid or one adsorbed on the NP surface. The value of T_{fus} can change significantly depending on the nanoparticle/nanopore size, the nature of the surface, etc. A lowering of T_{fus} typically occurs on silica materials, but on highly attractive surfaces like carbon or mica, an increase of T_{fus} can occur [6]. Gubbins et al. [7] reported that T_{fus} increased for organic substances interacting with MWCNT and decreased in the case of water on MWCNT and silica surfaces.

At a characteristic size of a few nanometers, thermal behavior of a nanoconfined liquid changes dramatically. A sigmoid heat-capacity curve with no trace of a melting peak has been observed for water adsorbed on the surface of nanosized rutile and anatase [8], as well as water [9, 10, 11],

benzene [12], toluene [13], methylcyclohexane [14], and *tert*-butylcyclohexane [14] confined in nanopores of silica materials.

In this work, densities were measured for the (IL + MWCNT) nanofluids prepared using alternative procedures. Thermal behavior of the [C₄mim]PF₆ + MWCNT system was studied over a wide range of compositions by adiabatic calorimetry. At high IL content, no size-specific anomalies were detected. At low IL content, a heat capacity curve similar to that previously reported for nanoconfined molecular liquids was observed. Possible explanations of the observed behavior are discussed.

2. Experimental

Stacked-cup type MWCNT (Vision Development, Japan) were used in this work. Structural characteristics of the material have been reported [15]. Prior to preparation of the composites, the samples were kept in a laboratory oven at $T = (393 \text{ to } 403) \text{ K}$ for several hours. The MWCNT treated in a similar way had the following elemental composition: $w(\text{C}) = (97.78 \pm 0.10) \cdot 10^{-2}$, $w(\text{H}) = (0.076 \pm 0.012) \cdot 10^{-2}$, $w(\text{N}) = (0.45 \pm 0.10) \cdot 10^{-2}$, $w(\text{Ni}) = (0.87 \pm 0.02) \cdot 10^{-2}$, $w(\text{O}) = (0.83 \pm 0.18) \cdot 10^{-2}$ [15].

The samples of the ILs used in this research are described in Table 1.

TABLE 1

Sample Table

Chemical name	Source	Initial purity specified by supplier	Purification method	Final mole fraction purity	Analysis method
[C ₄ mim]PF ₆ ^a	Merck	0.99	Evacuation	0.997	Fractional melting [16]
	Iolitec	0.995		N/A	
[C ₄ mim]BF ₄ ^b	Merck	0.99	Evacuation	N/A	
[C ₄ mim]NTf ₂ ^c	Iolitec	0.98	Evacuation	0.985	Fractional melting [17]
[C ₄ mPrl]NTf ₂ ^d	Merck	0.99	Evacuation	0.998	Fractional melting [18]

^a 1-butyl-3-methylimidazolium hexafluorophosphate^b 1-butyl-3-methylimidazolium tetrafluoroborate^c 1-butyl-3-methylimidazolium bis(trifluoromethanesulfonyl)imide^d 1-butyl-1-methylpyrrolidinium bis(trifluoromethanesulfonyl)imide

INFs were prepared using two different procedures. Procedure I was similar to that proposed by Fukushima et al. [19]. MWCNT and the IL were degassed and, then, mixed and ground in an agate mortar for 45 min. This technique resulted in low-density INFs, presumably because a significant part of the inner space of the MWCNT was not filled with IL [1]. To prepare high-density INFs, a second procedure (Procedure II) was developed. One half of the necessary IL was placed in a mortar, then the required amount of MWCNT was poured into the liquid, and the remaining IL was added to cover the MWCNT completely. The mortar was exposed to a vacuum of $p = 0.1$ kPa for 5 h to have ILs pulled into the core of the nanotubes. Then the components were ground for 45 min.

Preparation of INFs and further manipulations were carried out in a dry box. A typical yield was (1 to 2) g of the composite. If a larger mass of the composite was needed, several batches of known compositions were combined. The products prepared this way were viscous fluids with $w(\text{MWCNT}) < 0.25$. At higher mass fractions, a uniform fluid could not be obtained reproducibly because the system did not have enough IL to wet the MWCNT surface with the procedure used.

Even at $w(\text{MWCNT}) = 0.25$, the MWCNT internal volume is only large enough to absorb a few percent of ions, as demonstrated below. Therefore, to reveal potential effects due to nanosize, the bulk IL must be removed. To do that, 5 g of INF was washed several times with acetonitrile (Khimmed, $w = 0.999$), which had been treated with P_2O_5 and distilled. A major part of the liquid phase was decanted after each addition. After that, the remained acetonitrile was distilled at atmospheric pressure and then in vacuum until a constant mass of resulting black powder was achieved.

The density of INFs was measured near room temperature in a glass cylinder with a flat top. The volume of the cylinder V was calibrated with relative expanded uncertainty $U_r(V) = 0.0021$ ($k = 2$), using pure $[\text{C}_4\text{mim}]\text{BF}_4$, $[\text{C}_4\text{mim}]\text{PF}_6$, $[\text{C}_4\text{mim}]\text{NTf}_2$, and $[\text{C}_4\text{mPr}]\text{NTf}_2$ as reference liquids. Critically evaluated [20] densities were used for the reference liquids. The cylinder was gradually filled with the studied INF using a syringe. Thus, formation of bubbles or cavities was avoided. The fluid was leveled using a flat-top polypropylene piston. The cylinder was kept in a dry box for at least 20 minutes. The temperature was measured with a liquid-in-glass thermometer and remained constant over the measurement period within ± 1 K. The experiments were repeated 4 to 6 times. By exposing the filled cylinder to the air, it was found that the mass changes due to adsorption of gases from air could be neglected [1].

Heat capacities of the composites in the temperature range (80 to 370) K were measured in a TAU-10 adiabatic calorimeter (Termis, Moscow, Russia) [21]. The experimental procedures have been described [22]. Each heat-capacity determination involved initial measurement of temperature and its drift rate, as well as the electrical heating of the sample cell, which was followed by an equilibration period and measurement of the final temperature, adjusted for the background drift rate. Temperature was measured with a Fe/Rh resistance thermometer ($R_0 = 50 \Omega$) calibrated on ITS-90 by VNIIFTRI (Moscow).

For determination of normal heat capacity, heating periods, equilibration time, and periods for drift measurements were 400 s, (300 to 400) s, and 400 s, respectively. A temperature step of ~ 2 K was used. For the pre-melting region, thermal relaxation was observed for 1400 s, followed by measurement of the temperature drift for 1500 s in some series.

The samples of (1.2 to 1.4) g for the fluids and about 0.65 g for the powders were loaded into a calorimetric container of 1.1 cm^3 volume in a dry box. Outside of the phase-transition regions,

the heat capacity of a sample contributed (0.19 to 0.32) of the total heat capacity of the system for the powder samples and (0.47 to 0.57) for the fluids. The relative expanded uncertainty in the heat capacity measurements was estimated to be $U_r(c_p) = 0.004$ [22].

All sample masses were corrected for buoyancy. The reported uncertainties correspond to the 95 percent confidence interval for an assumed normal distribution (coverage factor $k = 2$) and include uncertainties due to repeatability, calibration, and thermostating.

3. Results and Discussion

3.1. Density

The experimental INF densities are given in Table 2. Generally, the densities of INFs prepared with Procedure I were lower than those made with Procedure II (Table 2). Also, if Procedure II was used, the apparent densities of MWCNT were significantly more consistent. It can be hypothesized that with Procedure II, the IL filled most of the MWCNT inner space. This statement is supported by the fact that the apparent densities of MWCNT for INFs prepared with this procedure were close to the density of graphite $\rho = 2265 \text{ kg}\cdot\text{m}^{-3}$ [23]. Normally, it is assumed that the vacuum treatment is not needed to have liquids inside hollow nanotubes, however, this is not the case for ILs. This behavior may be due to their high viscosity.

TABLE 2

Experimental densities ρ of INF with the MWCNT mass fraction w at temperature T and pressure $p = 99 \text{ kPa}$, derived apparent densities of MWCNT ρ^* , and their expanded uncertainties

$U (k \approx 2)$ ^a

IL	Procedure	w	T / K	$\rho / \text{kg}\cdot\text{m}^{-3}$	$\rho^* / \text{kg}\cdot\text{m}^{-3}$	$\Delta \rho^* / \text{kg}\cdot\text{m}^{-3}$ ^b
[C ₄ mim]BF ₄	I	0.1524	296.2	1287 ± 5	2110 ± 81	166 ± 73
[C ₄ mim]BF ₄	I	0.2338	296.9	1347 ± 3	2224 ± 35	52 ± 25
[C ₄ mim]NTf ₂	I	0.0693	294.2	1472 ± 3	2119 ± 83	126 ± 83
[C ₄ mim]NTf ₂	I	0.1484	293.7	1510 ± 3	2098 ± 38	147 ± 24
[C ₄ mPr1]NTf ₂	I	0.2391	295.2	1519 ± 6	2115 ± 47	153 ± 48
[C ₄ mim]PF ₆	I	0.045 to 0.302	293		2061 ± 37 [1]	153 ± 63
[C ₄ mim]BF ₄	II	0.2318	296.4	1350 ± 3	2276 ± 32	
[C ₄ mim]NTf ₂	II	0.2067	296.0	1553 ± 3	2245 ± 33	
[C ₄ mPr1]NTf ₂	II	0.2008	301.2	1509 ± 3	2268 ± 37	
[C ₄ mim]PF ₆	II	0.1665	291.4	1464 ± 4	2214 ± 55	

^a Standard uncertainties $u(w) = 1 \cdot 10^{-4}$, $u(T) = 0.5 \text{ K}$, $u(P) = 1 \text{ kPa}$. The uncertainty for the mass fractions considers only the contribution from weighing. The uncertainty due to the IL purity was not considered because the cylinder was calibrated using the same IL samples.

^b $\rho^*(\text{procedure II}) - \rho^*(\text{procedure I})$

The [C₄mim]PF₆ INFs prepared by Procedure I had the lowest apparent density of MWCNT among all considered INFs (Table 2). This extreme value can be used to estimate the average

internal diameter of a nanotube d_i . To do that, one need assume that, in this case, the IL does not penetrate the nanotubes. Then,

$$d_i = d_e \sqrt{\frac{\frac{1}{\rho_I} - \frac{1}{\rho_{II}}}{\frac{1}{\rho_I}}} = 15 \text{ nm}, \quad (2)$$

where the average external diameter of a nanotube $d_e = 50 \text{ nm}$ [15], ρ_I is the minimum apparent density of MWCNT in the INF prepared according to Procedure I and ρ_{II} is the average apparent density of MWCNT in the INF prepared according to Procedure II. The maximum absorption capacity of MWCNT for [C₄mim]PF₆ can be estimated as

$$w = \frac{d_i^2}{d_e^2 - d_i^2} \frac{\rho(\text{IL})}{\rho_{II}} = 0.06. \quad (3)$$

This means that 1 g MWCNT has enough internal space to contain 0.06 g [C₄mim]PF₆.

3.2. Adiabatic calorimetry

Five ([C₄mim]PF₆ + MWCNT) composites, including one reported earlier [1], were studied in an adiabatic calorimeter (Table 3). The samples differed by phase state, IL content, and preparative procedure.

The combination with MWCNT favored crystallization of the IL, and the studied fluid samples did not form a glass on cooling in the adiabatic calorimeter at an initial rate of $\sim 30 \text{ mK}\cdot\text{s}^{-1}$. This behavior differed from that of pure [C₄mim]PF₆, which crystallized only if the sample was vitrified and then heated to $T = 213 \text{ K}$. All three polymorphic sequences found for pure [C₄mim]PF₆ [16] were observed in INF. To keep consistency with our previous work [16], these sequences were designated as Sequence I, Sequence II, and Sequence III in order of their

appearance on continuous heating. Solid phases within a given sequence were distinguished by numeric indices (for example, crII₁). Sequence III had only one crystal phase crIII. One crystal phase crI was also detected in Sequence I [16] though other polymorphs of this sequence might exist.

TABLE 3

Samples of ([C₄mim]PF₆ + MWCNT) composites studied by adiabatic calorimetry ^a

Abbreviation	Appearance	w(MWCNT)	Preparative procedure
INF1	Fluid	0.1979 ± 0.0001	I
INF2	Fluid	0.2026 ± 0.0001	II
INF3	Fluid	0.1142 ± 0.0001 [1]	I
P1	Sticky powder	0.7913 ± 0.0014	II + CH ₃ CN wash-out
P2	Non-sticky powder	0.9171 ± 0.0014	II + CH ₃ CN wash-out

^a Expanded uncertainties are reported following the ± sign

For Sequences I and II, the heating to a certain temperature resulted in spontaneous crystal-to-crystal transformations and, therefore, accurate heat capacity values could not be obtained above this temperature (Figures 1 to 3, Tables S1 to S3). The measurements were continued in this region to follow the transformation processes and to identify the formed phases.

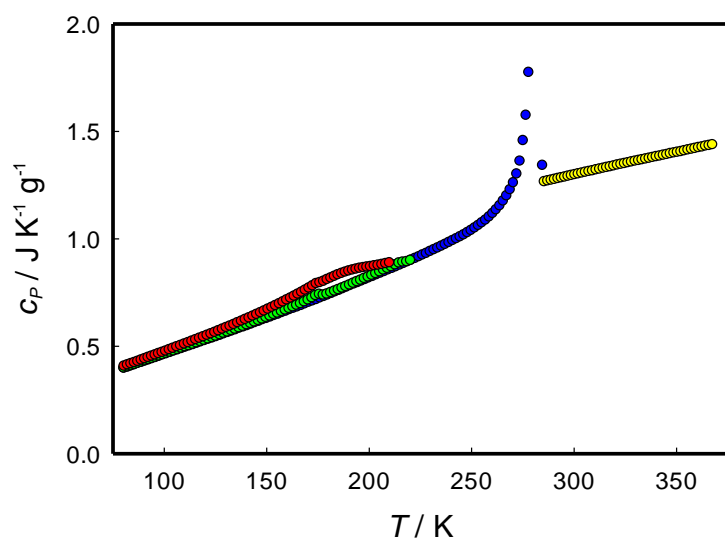


FIGURE 1. Experimental heat capacities of INF1. Colors are used to distinguish between the IL phase sequences: red, Sequence I (+ Sequence II); green, Sequence III + Sequence II; blue, Sequence III; yellow, liquid

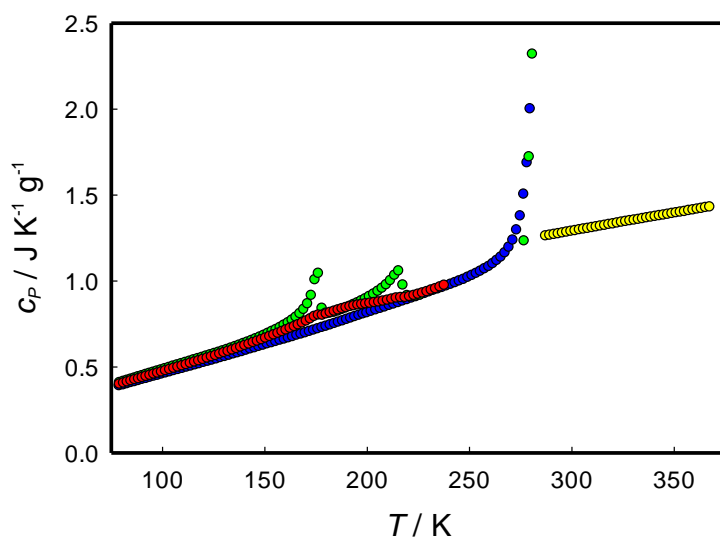


FIGURE 2. Experimental heat capacities of INF2. Colors are used to distinguish between the IL phase sequences: red, Sequence I (+ Sequence II); green, Sequence II; blue, Sequence III; yellow, liquid

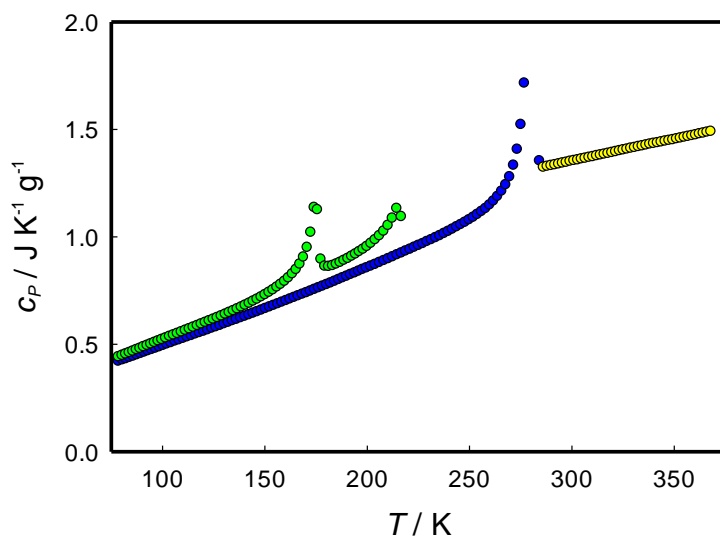


FIGURE 3. Experimental heat capacities of INF3. Colors are used to distinguish between the IL phase sequences: green, Sequence II; blue, Sequence III [24]; yellow, liquid [16]

INF1. On cooling this fluid from 310 K, the $[C_4mim]PF_6$ phases of Sequence I formed (Figure 1). The crystals obtained this way had an admixture of the Sequence II polymorphs, as indicated by a minor peak at $T = 174$ K characteristic to this sequence [16]. During the measurements, heat evolution started at $T \approx 210$ K and, if the experiments were continued, ended at $T = 275$ K. When the exothermic process was stopped at $T = 270$ K by cooling the sample, a mixture of polymorphs belonging to Sequences II and III was obtained. This mixture became unstable during the measurements at $T > 220$ K, as evidenced by heat evolution. The melting curves obtained in these calorimetric series had a shoulder after the main peak similar to the one observed for the pure IL [16]. The peak and shoulder corresponded to melting of crIII and crII₄, respectively.

If the sample was cooled after the exothermic transformation described above had ended ($T > 275$ K), the formed crystals of Sequence III did not have a detectable admixture of other polymorphs. These crystals were stable to T_{fus} at the time scale of the measurements.

INF2. A sigmoid heat capacity curve that can be assigned to Sequence I was observed for the sample cooled from $T = 320$ K. Small anomalies at $T = 174$ K and 216 K indicated a small admixture of crystals from Sequence II (Figure 2). During the measurements, an exothermic effect started at $T \approx 240$ K and, finally, resulted in formation of more stable polymorphs. This transformation was completed at $T \approx 280$ K. Normally, a mixture of crystals from Sequences II and III was formed in this process. As for pure IL [16], two temperatures of fusion for $[\text{C}_4\text{mim}]\text{PF}_6$ (Figure 4) corresponding to crIII and crII₄ were observed.

To obtain crystals of Sequence II with no notable admixture of Sequence III, the partially melted sample was kept at $T = (283.7 \text{ to } 283.9)$ K for 13 h. The melting curve for this sample (Figure 4) shows a single peak corresponding to the melting of crII₄. This crystal was kinetically stable on cooling to $T = 77$ K and for performing the measurements outside the temperature range $T = (226 \text{ to } 276)$ K, where the transformation into Sequence III occurred. Thus, the heat capacity of the INF that contained the crystals of Sequence II was obtained in the temperature ranges of (78 to 226) K and (276 to $T_{\text{fus}}(\text{crII}_4)$) (Figure 2).

Annealing at $T = 280$ K resulted in formation of the crystals of Sequence III, which were stable during the measurements up to $T = 283.2$ K that is a few tenths of kelvin lower than its triple-point temperature.

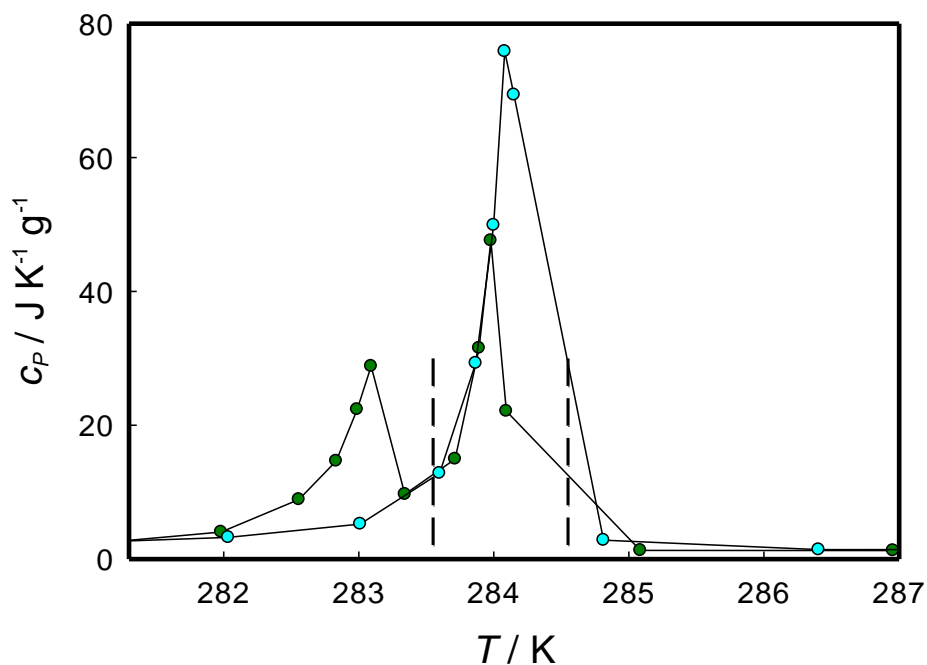


FIGURE 4. Typical melting curves for INF2: green, right after the exothermal process at $T = (240 \text{ to } 280) \text{ K}$; cyan, annealed at $T = (283.7 \text{ to } 283.9) \text{ K}$. The first peak was assigned to melting of crIII, the second one was assigned to crII₄, - - - are corresponding triple-point temperatures determined earlier. [16] The line is a guide for the eye. Uncertainties for the heat capacities are large due to long equilibration times that precluded high-precision measurements in this region.

INF3. Sequences II and III were observed for this INF (Figure 3). The crystals of Sequence II spontaneously transformed into those of Sequence III at $T > 215 \text{ K}$. The melting was observed only for crIII. Near the melting point, the admixture of crII₄ in crIII was not significant.

Previously [1], the heat capacity of Sequence II was measured for the material without annealing.

To improve the data quality, an additional series of measurements was carried out (Figure 3).

Prior to this series, after the crystallization had begun at $T = 268 \text{ K}$, the sample was naturally

heated to $T=274$ K and was annealed at this temperature for 4 h to minimize the presence of other polymorphs.

The apparent heat capacities of $[\text{C}_4\text{mim}]\text{PF}_6$ (Figs. 5 to 7) were calculated with eq. (1) using the MWCNT heat capacities from Ref. [1]. Outside the phase-transition ranges, the apparent heat capacities of IL crystals for all INFs were consistent with those of bulk IL within $\pm 5 \cdot 10^{-3} C_{P,m}$. The phase-transition peaks for INFs were wider, while the $C_{P,m}$ maxima were significantly lower.

The differences between enthalpies of the $\text{crII}_1 = \text{crII}_2$ transition ($T_{\text{tr}} = 174$ K) in INFs and the respective value for the bulk IL were not statistically significant. The enthalpy of fusion for Sequence III (Table S6) was 18.67 ± 0.19 , 18.42 ± 0.18 , and 18.94 ± 0.19 $\text{kJ}\cdot\text{mol}^{-1}$ for INF1, INF2, and INF3, respectively, as compared to $\Delta_{\text{crIII}}^1 H_{\text{m}} = 19.60 \pm 0.02$ $\text{kJ}\cdot\text{mol}^{-1}$ [24] for the pure IL. A possible explanation of the lower enthalpies is that a portion of the IL close to the MWCNT interface does not exhibit a first-order transition peak associated with melting. With this assumption, the fraction of this IL is estimated to be from 0.03 in INF3 to 0.06 in INF2.

The apparent heat capacities for the liquid $[\text{C}_4\text{mim}]\text{PF}_6$ in INFs (Figure 8) are lower than the bulk liquid $C_{P,m}$ by about $5 \cdot 10^{-3} C_{P,m}$ over the temperature range (283 to 370) K, which is not statistically significant.

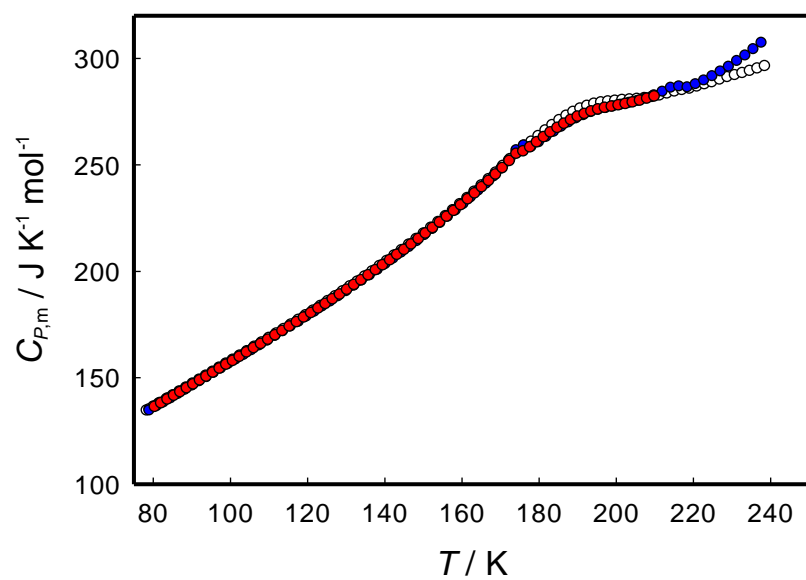


FIGURE 5. Apparent heat capacities of Sequence I of $[\text{C}_4\text{mim}]\text{PF}_6$ obtained from the data on: red, INF1; blue, INF2; white, pure IL

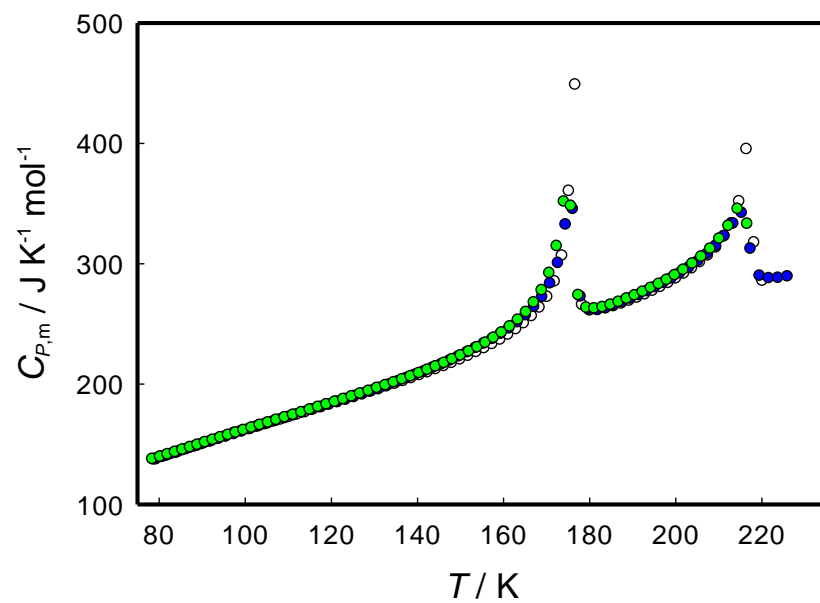


FIGURE 6. Apparent heat capacities of Sequence II of $[\text{C}_4\text{mim}]\text{PF}_6$ obtained from the data on: red, INF1; blue, INF2; green, INF3; white, pure IL

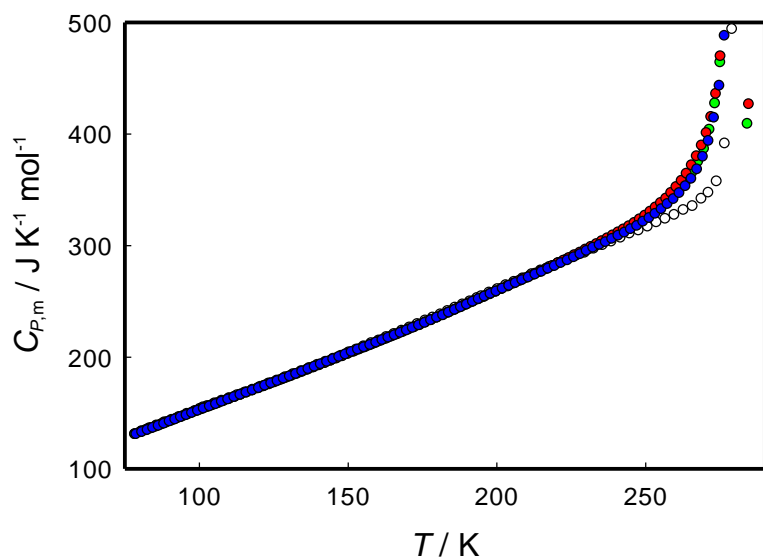


FIGURE 7. Apparent heat capacities of Sequence III of $[\text{C}_4\text{mim}]\text{PF}_6$ obtained from the data on: red, INF1; blue, INF2; green, INF3; white, pure IL

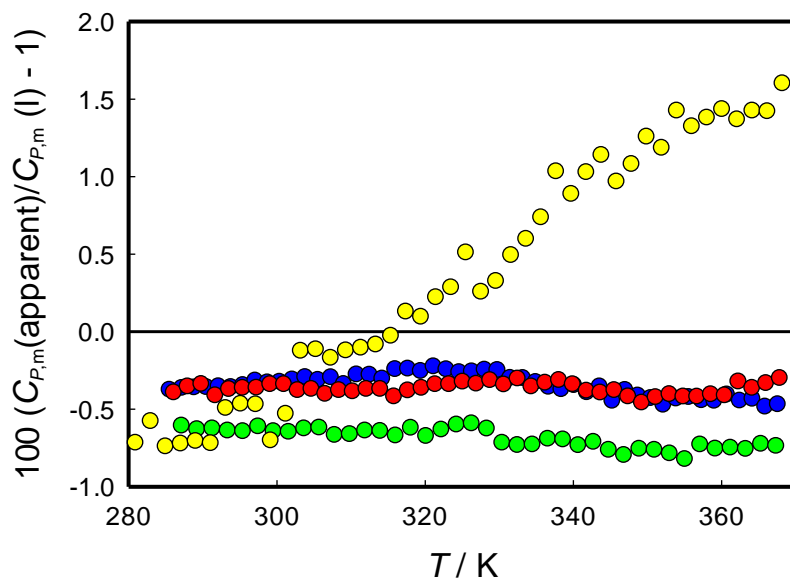


FIGURE 8. Deviation of the apparent heat capacities of liquid $[\text{C}_4\text{mim}]\text{PF}_6$ from the heat capacity of pure IL: red, INF1; blue, INF2; green, INF3; yellow, P1

PI. The heat capacity curves of the powder-like composites (Figures 9 and 10, Tables S4 and S5) significantly differed from those of the fluid samples. When P1 was cooled to $T = 77$ K, [C₄mim]PF₆ partially vitrified. The heat-capacity change at the glass transition near $T = 190$ K was significantly smaller than that of the bulk IL (Figure 10). Annealing at $T = 217$ K for 13 h resulted in partial crystallization that revealed itself with a decreased height of the glass-transition-like step. The remaining part is associated with the reversible transformations between the crystal-like and liquid-like regions at the MWCNT interface, as discussed below.

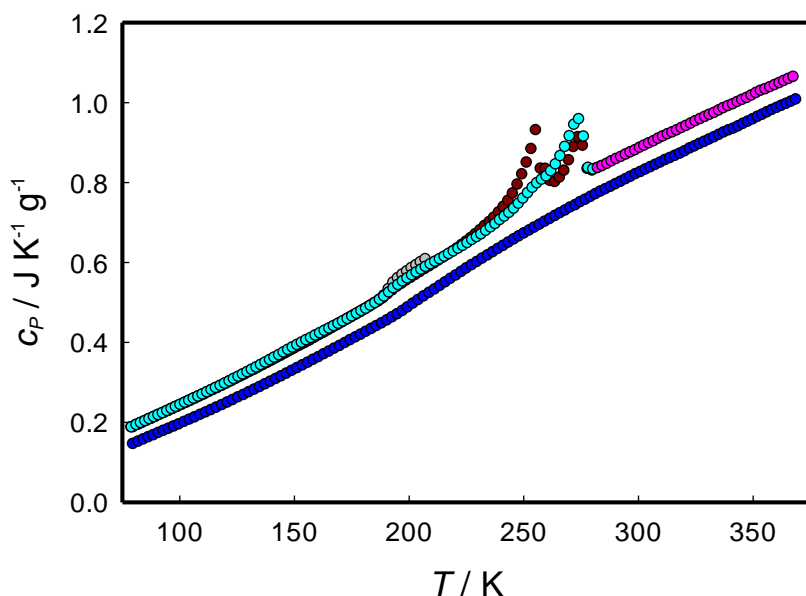


FIGURE 9. Experimental heat capacities of powder-like composites: pink, P1 after heating to 370 K and cooling to $T = 285$ K; gray, P1 after heating to 370 K and cooling to $T = 77$ K; brown, P1 annealed at $T = 217$ K; cyan, P1 annealed at $T = 265$ K; blue, P2

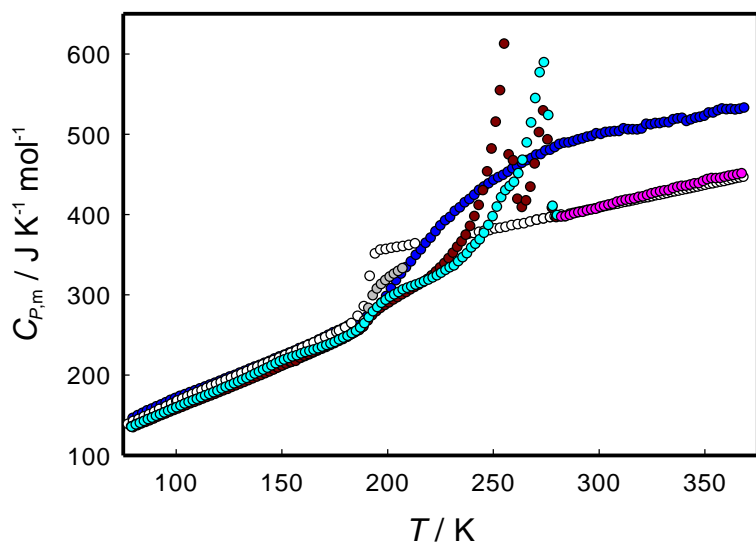


FIGURE 10. Apparent heat capacities of $[\text{C}_4\text{mim}]\text{PF}_6$ obtained from the experimental data on powder-like composites: pink, P1 after heating to 370 K and cooling to $T = 285$ K; gray, P1 after heating to 370 K and cooling to $T = 77$ K; brown, P1 annealed at $T = 217$ K; cyan, P1 annealed at $T = 265$ K; blue, P2; empty circles, glass and liquid of bulk IL

After this annealing, a peak at $T = (255 \pm 1)$ K followed by a shoulder and another peak at $T = (274 \pm 1)$ K appeared in the heat-capacity curve. The measurements were accompanied by an exothermic effect right after the first peak, as detected by the positive temperature drifts. This means that different polymorphs were simultaneously present in the sample.

P1 treated as described above was annealed at $T = 265$ K for 6 h and then cooled down. Only the increased peak at $T = (273 \pm 1)$ K accompanied by a shoulder at about 255 K remained. No exothermal effect could be detected. This peak corresponds to melting of an unknown polymorph. Since the peak temperature is significantly lower than T_{fus} of crIII and crII₄ observed in INF (Figure 4), it is hard to determine the sequence to which it belongs. It might be the

melting of bulk crI whose T_{fus} has been estimated to be 274 ± 8 K [16]. Another option is the melting of nanoconfined crIII or a new phase.

The apparent heat capacity of the liquid [C₄mim]PF₆ in P1 (Figure 8) is close to the bulk value near $T = 280$ K and is about $0.015C_{P,m}$ higher near $T = 370$ K, which is close to the expected uncertainty

P2. The heat-capacity curve for P2, which had the highest MWCNT content, did not have any traces of the [C₄mim]PF₆ crystal phases (Figure 10). Unlike P1, the sigmoidal anomaly starting at $T = 190$ K was not hidden by phase transitions. This feature extended to $T = 280$ K, which was close to the melting-point temperatures of the bulk IL polymorphs.

Boerio-Goates et al. [8] reported a similar behavior for the “outer” water adsorbed on the surface of 7 nm TiO₂ (rutile and anatase). Nagoe et al. observed a sigmoid-shaped heat capacity curve with no peaks for water confined in the (1.5 and 1.7) nm diameter pores of MCM-41 [9] and for ordinary and heavy water in the 1.1 nm diameter silica gel voids [10]. This curve was interpreted as a combination of three glass transitions associated with different numbers of the breaking hydrogen bonds [9]. Later, Tombari et al. [11] revised this interpretation. Based on the high-accuracy temperature-modulated DSC measurements, they concluded that the sigmoidal anomaly in the heat capacity of water was due to gradual reversible transformations between the distorted ice-like structures and liquid-like ones.

Nagoe et al. [12] determined heat capacities of benzene confined in silica MCM-41 nanopores of different diameters. They demonstrated that a similar anomaly observed at pore diameter $d < 3.3$ nm was not associated with the glass transition. Instead, they detected two relaxation processes on the hump and one at its low-temperature side. The processes on the hump were tentatively assigned to (i) droplet breaking, film thinning, and (ii) arrangement of droplets and films. A

similar shaped heat-capacity curve was reported for toluene confined in nanoporous MCM-41 and/or SBA-15 (the exact material was not specified) [13], and methylcyclohexane and tert-butylcyclohexane confined in 1.1 nm silica gel voids [14].

Thus, the interpretation by Tombari et al. [11] who associated the observed heat-capacity anomaly with gradual transformation of the crystal-like structures to liquid-like ones seems to be valid for the systems studied in this work as well.

The MWCNT used in this work had an average internal diameter of 15 nm, as estimated with eq. (2). This parameter is rather high for the discussed phenomenon that occurred at the pore diameter < 2 nm for water and < 3.3 nm for benzene. However, if one considers a significantly larger size of the $[C_4mim]PF_6$ ionic pairs, this behavior does not look anomalous.

At $T > 280$ K, the apparent heat capacity of $[C_4mim]PF_6$ in P2 is $0.2C_{P,m}$ higher than that of the bulk IL (Figure 10). In this temperature range the expanded uncertainty was estimated to be $U(C_{P,m}) = (0.05 \text{ to } 0.07)C_{P,m}$, therefore, this difference is statistically significant. The heat capacity curve has about the same slope as that for the bulk IL.

The heat capacity of “outer” water adsorbed on the anatase particles was larger than that for the bulk at $T > T_{fus}$ [8]. The results for water confined in the silica materials [9, 10, 11] were inconsistent. No significant increase in $C_{P,m}$ was observed for the 1.5 nm and 1.7 nm pore-MCM-41 [9]. The heat capacity of water confined in the 1.4 nm and 1.8 nm pore-MCM-41-S at $T = 280$ K was higher than the bulk value by 10 % and 6 %, respectively [11]. For ordinary and heavy water confined in the 1.1 nm silica gel voids, the heat capacity was larger than the bulk one [10]. Also, in Refs. [11] and [10], the heat capacity curves of the nanoconfined water were approximately parallel to that of the bulk.

A similar heat-capacity increase was observed for benzene confined in MCM-41 [12] and toluene confined in silica nanopores [13]. Nagoe et al. [12] explained the excess heat capacity as partial vaporization of the liquid. Morineau et al. [13] suggested this difference was due to extra modes at the interface between the matrix and the liquid, adsorption enthalpy, or a change in the matrix contribution itself when filled. Since the measurements [13] were carried out for sample masses of (0.3 to 0.5) g in a 5 cm³ container, the vaporization explanation cannot be excluded. The apparent heat capacities of nanoconfined alkylcyclohexanes [14] were somewhat lower than the bulk values even at $T > T_{\text{fus}}$ for the bulk. Thus, these results do not allow one to conclude whether the heat capacity of the nanoconfined liquid changes relative to the bulk value.

Vaporization cannot explain the observed behavior of $C_{P,m}$ above T_{fus} , since [C₄mim]PF₆ has a very low volatility in the studied temperature range. An error in the composition is also not an option: reduction of the right-hand part of the $C_{P,m}$ curve to the bulk value would make the left-hand part unphysically low. The heat capacity of the liquid phase is normally higher than that of the crystal. It is difficult to propose a physical mechanism, which would explain an increase of the bulk liquid heat capacity by about 90 J·K⁻¹·mol⁻¹ in the nanoconfinement.

All calculations above are based on eq. (2) and the assumption that the heat capacity of MWCNT does not change when mixed with the IL. However, this assumption cannot be verified. If the heat capacity of MWCNT is larger than the value for pure MWCNT by (1.03 to 1.04) $C_{P,m}$ at $T = (280 \text{ to } 370) \text{ K}$, the unexpectedly high apparent heat capacity of IL becomes close to the bulk $C_{P,m}$. This seems to be physically plausible. If the liquid fills a nanotube, it will be damping the lattice vibrations. Therefore, the corresponding frequencies will decrease, which will result in an increased heat capacity. This increase should occur only at relatively high temperatures. At low temperatures, because of thermal expansion, the interface area between the ions and the

MWCNT walls will be significantly smaller. Also, the IL particles will be frozen. Thus, the resulting effect on the heat capacity will be significantly weaker. Further studies are needed to support this explanation.

4. Conclusion

The densities of INF prepared using Procedure II were found to be higher and more reproducible than those of INF obtained according to Procedure I. The principal difference between the procedures is evacuation of the IL + MWCNT mixture immediately before grinding.

The ($[\text{C}_4\text{mim}]\text{PF}_6 + \text{MWCNT}$) composites were studied by adiabatic calorimetry. At $w(\text{MWCNT}) = 0.1$ to 0.2 , all polymorphs characteristic of the bulk $[\text{C}_4\text{mim}]\text{PF}_6$ were identified. The specific heat capacity was found to be an additive quantity of specific heat capacities of the components for the crystal and liquid phases. The only difference in phase transition parameters relative to those of the bulk IL was a slightly decreased melting enthalpy for crIII.

For the powder-like sample with $w(\text{MWCNT}) = 0.79$, heat-capacity peaks were found that had not been observed for the fluid samples or bulk IL. For both powder-like samples, the heat capacity curve had a sigmoidal shape. Similar behavior due to gradual transformation from the crystal-like domains to liquid-like ones had been reported for nanoconfined molecular liquids.

The heat capacity of NP should be larger than that of pure MWCNT to explain the increased heat capacity of the composites above room temperature.

5. Notes

The authors declare no competing financial interest.

Acknowledgement

This article is, in part, a contribution of NIST, and is not subject to copyright in the United States. Trade names are provided only to specify procedures adequately and do not imply endorsement by the National Institute of Standards and Technology. Similar products by other manufacturers may be found to work as well or better.

Appendix A. Supplementary data

Supplementary data associated with this article can be found, in the online version, at ...

References

1. M. P. Shevelyova, Y. U. Paulechka, G. J. Kabo, A. V. Blokhin, A. G. Kabo, *J. Phys. Chem. C* 117 (2013) 4782-4790. DOI: 10.1021/jp3059432.
2. J. Liu, F. Wang, L. Zhang, X. Fang, Z. Zhang, *Renewable Energy* 63 (2014) 519-523. DOI: 10.1016/j.renene.2013.10.002.
3. T. C. Paul, AKM M. Morshed, J. A. Khan, *Procedia Engineering* 56 (2013) 631-636. DOI: 10.1016/j.proeng.2013.03.170.
4. K. Oster, C. Hardacre, J. Jaquemin, A. P. C. Ribeiro, A. Elsinawi, *J. Mol. Liq.* 253 (2018) 326-339. DOI: 10.1016/j.molliq.2018.01.025.
5. Y. U. Paulechka, *J. Phys. Chem. Ref. Data* 39 (2010) 033108. DOI: 10.1063/1.3463478.
6. C. Alba-Simionesco, B. Coasne, B., G. Dosseh, G. Dudziak, K. E. Gubbins, R. Radhakrishnan, M. Sliwinska-Bartkowiak, *J. Phys.: Condens. Matter* 18 (2006) R15–R68. DOI: 10.1088/0953-8984/18/6/R01.
7. K. E. Gubbins, Y. Long, M. Śliwinska-Bartkowiak, *J. Chem. Thermodyn.* 74 (2014) 169-183. DOI: 10.1016/j.jct.2014.01.024.
8. J. Boerio-Goates, G. Li, L. Li, T. F. Walker, T. Parry, B. F. Woodfield, *Nano Lett.* 6 (2006) 750-754. DOI: 10.1021/nl0600169.
9. M. Oguni, Y. Kanke, A. Nagoe, S. Namba, *J. Phys. Chem. B* 115 (2011) 14023-14029. DOI: 10.1021/jp2034032.
10. M. Oguni, S. Maruyama, K. Wakabayashi, A. Nageo, *Chem. Asian J.* 2 (2007) 514-520. DOI: 10.1002/asia.200600362.
11. E. Tombari, G. Salvetti, G. P. Johari, *J. Phys. Chem. B* 116 (2012) 2702-2709. DOI: 10.1021/jp209598x.

-
12. A. Nagoe, M. Oguni, H. Fujimori, *J. Phys.: Condens. Matter* 27 (2015) 455103. DOI: 10.1088/0953-8984/27/45/455103.
 13. D. Morineau, Y. Xia, C. Alba-Simionesco, *J. Chem. Phys.* 117 (2002) 8966-8972. DOI: 10.1063/1.1514664.
 14. S. L. L. M. Ramos, M. Ogino, M. Oguni, *J. Phys.: Condens. Matter* 27 (2015) 035103. DOI: 10.1088/0953-8984/27/3/035103.
 15. G. J. Kabo, E. Paulechka, A. V. Blokhin, O. V. Voitkevich, T. Liavitskaya, A. G. Kabo, *J. Chem. Eng. Data* 61(2016) 3849-3857. DOI: 10.1021/acs.jced.6b00525.
 16. E. Paulechka, T. Liavitskaya, A. V. Blokhin, *J. Chem. Thermodyn.* 102 (2016) 211-218. DOI: 10.1016/j.jct.2016.07.012.
 17. A. V. Blokhin, Y. U. Paulechka, A. A. Strechan, G. J. Kabo, *J. Phys. Chem. B* 112 (2008) 4357-4364. DOI: 10.1021/jp710872s.
 18. Y. U. Paulechka, A. G. Kabo, A. V. Blokhin, G. J. Kabo, M. P. Shevelyova, *J. Chem. Eng. Data* 55 (2010) 2719-2724. DOI: 10.1021/je900974u.
 19. T. Fukushima, A. Kosaka, Y. Ishimura, T. Yamamoto, T. Takigawa, N. Ishii, T. Aida, *Science* 300 (2003) 2072-2074. DOI: 10.1126/science.1082289.
 20. NIST ThermoData Engine Version 10.3 – Pure Compounds, Binary Mixtures and Reactions. NIST Standard Reference Database 103b, Gaithersburg, MD, 2018.
<https://www.nist.gov/mml/acmd/trc/thermodata-engine/srd-nist-tde-103b>, accessed: September 3, 2018.
 21. F. Pavese, V. M. Malyshev, *Advances Cryog. Eng.* 40(1994) 119-124.
 22. A. V. Blokhin, G. J. Kabo, Y. U. Paulechka, *J. Chem. Eng. Data* 51 (2006) 1377-1388. DOI: 10.1021/je060094d.

23. J. Y. Howe, C. J. Rawn, L. E. Jones, H. Ow, Powder Diffraction 18 (2003) 150-154. DOI:

10.1154/1.1536926.

24. G. J. Kabo, A. V. Blokhin, Y. U. Paulechka, A. G. Kabo, M. P. Shymanovich, J. W. Magee,

J. Chem. Eng. Data 49 (2004) 453-461. DOI: 10.1021/je034102r.